

# Measurement noise scaling laws for cellular representation learning

**Gokul Gowri**<sup>1, 3\*</sup><sup>†</sup>, **Igor Sadalski**<sup>2†</sup>, Dan Raviv<sup>2</sup>, Peng Yin<sup>1</sup>,  
Jonathan Rosenfeld<sup>2</sup>, Allon Klein<sup>1\*</sup>

<sup>1</sup>Department of Systems Biology, Harvard Medical School, Boston, MA, USA.

<sup>2</sup>Somite Therapeutics, Boston, MA, USA.

<sup>3</sup>Laboratory for Information and Decision Systems, Massachusetts Institute of Technology, Cambridge, MA, USA.

\*Corresponding author(s). E-mail(s): [gokulg@mit.edu](mailto:gokulg@mit.edu); [allon\\_klein@hms.harvard.edu](mailto:allon_klein@hms.harvard.edu);

†These authors contributed equally

## Abstract

Large genomic and imaging datasets can be used to fit models that learn representations of cellular systems, extracting informative structure from data. In other domains, model performance improves predictably with dataset size, providing a basis for allocating data and computation. In biological data, however, performance is also limited by measurement noise arising from technical factors such as molecular undersampling or imaging variability. By learning representations of single-cell genomic and imaging data, we show that noise defines a distinct axis along which performance improves predictably across tasks. This scaling follows a simple logarithmic law that is consistent across model types, tasks, and datasets, and can be derived quantitatively from a model of noise propagation. We identify robustness to noise and saturating performance as properties that vary across models and tasks. Applied to a 12-million-cell mouse embryogenesis dataset, a large Transformer-based model shows greater robustness but lower saturating performance than a variational autoencoder-based model.

**Keywords:** scaling laws, single-cell analysis

## <sup>1</sup> Introduction

Cellular profiles obtained by single-cell RNA sequencing (scRNA-seq) and high-content imaging now span diverse tissues, developmental stages, disease states, and experimental perturbations [1, 2]. These large datasets (collectively  $> 10^8$  samples) create opportunities to identify shared cellular states across experimental contexts and predict responses to novel perturbations [3, 4]. To realize these opportunities, representation learning models are used to capture biologically meaningful variation, while filtering out technical nuisance factors [5]. Several deep learning approaches underlie such models to date, including transformer-based architectures, autoencoder-based architectures, and contrastive losses [6–9].

9 In domains outside of biology including natural language processing, image processing and chemical  
10 informatics, large model development has been guided by the study of model scalability. Choices in  
11 architecture, data collection efforts, and training strategies are guided by deep learning scaling laws,  
12 which are empirical relationships that describe how model performance improves with increases in key  
13 resources like data, compute, and model parameters [10–15].

14 In biology, model performance can also be limited by noise in the data used for model training. A  
15 few specific data modalities, such as DNA sequence, exist in large repositories with reasonably low error  
16 rates ( $< 10^{-2}$  errors/nucleotide, [16]) but the majority of biological data modalities are more prone  
17 to measurement noise. scRNA-Seq and spatially-resolved transcriptomics, for example, are methods  
18 fundamentally limited by the low numbers of mRNA molecules per gene per cell. Though measurement  
19 sensitivity is increasing with ongoing development of these methods [17], for many existing technologies  
20 the probability of detecting a given mRNA molecule is well below 50%, and in some cases the detection  
21 rate is further decreased by insufficient sequence depth [18]. As a result, measured transcript counts are  
22 subject to undersampling noise. Fluorescent microscopy imaging is also prone to noise of different types  
23 including background signal, quantum yield and resolution [19].

24 In contrast to the scaling of model performance with data set size and model size, much less is known  
25 about the role of measurement noise on the ability of a model to learn meaningful representations.  
26 In textual representation by large language models (LLMs), errors in training data lead to degraded  
27 performance, even in the limit of infinite data [20]. However, textual data used in LLM training are much  
28 less noisy than biological data. As representation models are being developed for diverse biological tasks,  
29 understanding how noise alters the learning rate of models could be important.

30 Here, we recapitulate sample-size scaling in the quality of learned representations of scRNA-Seq,  
31 spatial transcriptomics and image data, and we show evidence for a general and quantitative scal-  
32 ing relationship between measurement noise and model performance. To show this law, we introduce  
33 an information-theoretic framework for studying the scalability of representation learning models with  
34 respect to changes in measurement noise and dataset size. We show that the noise-scaling law can be  
35 derived by analogy to additive Gaussian noise channels, and that the resulting theoretical framework can  
36 be used to guide experimental design. When applied to a 12-million-cell mouse embryogenesis dataset  
37 [21], our framework suggests that a Transformer-based model is more robust to noise, but has lower  
38 saturating performance than a variational autoencoder-based model.

39 **Results**

40 **A metric for representation-learning model performance**

41 In neural scaling analyses, it is typical to evaluate the quality of models directly by evaluating their loss  
42 in reconstructing test data [10–12, 14]. However, model loss is not comparable between model families,  
43 or even for a single model applied to data with different statistical properties [22] such as different  
44 noise properties. Therefore, to study the effect of noise on representation learning model performance,  
45 we introduced an alternative approach to measuring representation quality, by estimating the mutual  
46 information (MI) between the representations learnt by a model and some information about each sample  
47 that remains hidden until after learning is completed. Formally, this approach is a generalization of  
48 linear probing [23, 24], which estimates MI between a representation and a classification label. Our  
49 generalization uses a neural network-based estimator of MI that accommodates high-dimensional and  
50 continuous auxiliary signals[25]. This approach provides a performance metric that is comparable between  
51 model types and noise levels in a given data set.

52 We evaluated representation model performance for four test data sets, each of which provides single  
53 cell transcriptional state with some additional auxiliary signal as follows:

- 54 1. **Developmental time**, using an atlas of  $\sim 10^7$  cells profiled by scRNA-seq across mouse development  
55 where developmental time is quantified by embryonic stage [21].
- 56 2. **Surface protein abundances** of  $\sim 10^5$  peripheral mononuclear blood cells (PBMCs) measured by  
57 an antibody panel through CITE-seq [26].
- 58 3. **Transcriptional profile of a clonally related cell** in  $\sim 10^5$  mouse hematopoietic stem cells  
59 measured using lineage-traced scRNA-seq [27].
- 60 4. **Transcriptional profile of a spatially adjacent cell** in a coronal mouse brain section of  $\sim 10^5$   
61 cells measured using MERFISH [28].

62 For each of these, we evaluated two linear baselines: random projection and dimensionality reduction  
63 by principal component analysis (PCA), and we compared these to two modern generative models: single  
64 cell variational inference (SCVI) [29] and Geneformer [6]. SCVI is a variational autoencoder designed to  
65 compress high-dimensional gene expression information into a low-dimensional latent space. Geneformer  
66 instead uses a Transformer-based language model that maps gene expression vectors to sequences by  
67 ordering gene-specific tokens based on expression level.

68 In all cases, to facilitate consistent comparisons, we learned representations on one data subset, and  
69 then evaluated performance in a separate, fixed held-out subset. This approach ensures that observed  
70 differences in mutual information are attributable to variations in the representations themselves, rather  
71 than estimation artifacts.

72 **Cell number scaling for cellular representations**

73 As a baseline for understanding the impact of noise on model learning, we first tested whether auxiliary-  
74 MI performance,  $I$ , shows expected scaling behavior with the number of samples  $N$  – here, single cells  
75 – used in training. In large language models, performance scales as a power of sample number [14], and  
76 a similar law is seen for cell representation models [30]. We indeed found that  $I$  is well-described by  
77 a saturating power-law across all deep learning models and auxiliary tasks,  $I(N) = I_\infty - (N/N_{sat})^{-s}$ ,  
78 where the parameters  $I_\infty, N_{sat}, s$  characterize how each model learns from new data (fit residual sum of  
79 squares  $R^2 = 0.913 \pm 0.008$  across  $n = 44$  model and task combinations). The fits are shown collectively  
80 across models and datasets in **Fig. 1.b**, with parameter values and model comparisons in **Fig. 1.c**.

81 **Noise scaling for cellular representations**

82 Although deep learning models are colloquially thought to be strong denoisers, the degree to which cel-  
83 lular representation learning models are robust to noise in their training data is unknown. A noise robust  
84 model would exhibit a regime in which the informativity of learned representations remains stable despite  
85 increasing noise levels. We evaluated the extent to which models are noise robust by simulating increas-  
86 ing measurement noise through downsampling observed transcript counts, and subsequently evaluating  
87 the quality of the learned representations using auxiliary-MI performance.

88 The dependence of model performance  $I$  on the degree of downsampling noise is shown in **Fig. 1d**.  
89 As expected, reducing the depth per cell degrades the performance of all models, across all datasets.  
90 Of note, no model or dataset exhibits large regimes of noise robustness. Instead, many of the measured  
91 performance curves are sigmoidal, indicating only limited robustness at the transcript levels present in  
92 the original datasets before performance steadily deteriorates (**Fig. 1d**). A subset of the curves show a  
93 ‘hockey-stick’ shape, indicating negligible robustness to downsampling noise, even at full transcript levels.

94 Neural scaling laws provide expectations for how model performance improves with additional com-  
95 putational or data resources. Loss of representation quality as a function of downsampling noise produces  
96 families of smooth, sigmoidal performance curves, suggesting that a similarly simple quantitative rela-  
97 tionship might capture how measurement noise constrains biological representation learning. Such a  
98 relationship would be valuable for experimental design, enabling principled allocation of sequencing depth  
99 and cell numbers in the same way that neural scaling laws guide resource decisions in large-scale machine  
100 learning.

101 To investigate whether the observed noise–performance behavior is predictable, we turned to a clas-  
102 sical model of information loss in noisy communication channels (see **Box 1**). This framework extends  
103 established information-theoretic results [31] to derive an analytical relationship between the signal-to-  
104 noise ratio of a measurement,  $\eta = \text{SNR}$ , and the mutual information preserved about an underlying

105 external variable. This analysis (Eq. 2 in Box 1) yields a closed-form prediction for how auxiliary-MI  
106 performance should depend on sequencing depth:

$$\mathcal{I}(\alpha) = \mathcal{I}_{\max} - \frac{1}{2} \log \frac{\eta^2/\bar{\eta}^2 + 1}{\eta^2/\bar{\eta}^2 + 2^{-2\mathcal{I}_{\max}}}, \quad (1)$$

107 where  $\mathcal{I}_{\max}$  is the maximal information that can be extracted from a noiseless measurement at a fixed  
108 sample size, and  $\bar{\eta}$  serves as a measure of noise robustness (specifically, the signal-to-noise ratio at which  
109 a model can gain at most 1/2 a bit of information by increasing measurement sensitivity). To connect  
110 this general relationship to cellular measurements, we note that the signal-to-noise ratio introduced by  
111 molecular undersampling follows Poisson statistics,  $\eta^2 = \text{CV}^{-2} \propto \text{UMI}$  [32], and  $\bar{\eta}$  then takes on units  
112 of UMIs per cell.

113 In Fig. 1d, the theoretical curves defined by Eq. (1) (dotted lines) closely match the empirical perfor-  
114 mance curves (scatter points) across models and datasets. Strikingly, the noise-scaling relationship holds  
115 across model architectures and across single-cell datasets spanning nearly five orders of magnitude in  
116 sample size. When rescaled by their fitted  $\mathcal{I}_{\max}$  and  $\bar{\eta}$  values, empirically measured curves from all the  
117 model families collapse onto a single universal relationship, indicating that a shared principle governs  
118 how measurement noise in transcriptomic data limits representation learning.

119 The fitted noise-scaling parameters from Eq. 1 provide a compact summary of the noise-robustness of  
120 a model. In particular,  $\bar{\eta}$  reflects each model’s effective noise tolerance, while  $\mathcal{I}_{\max}$  captures its asymptotic  
121 capacity in the absence of measurement noise. For a given auxiliary task, models that combine low  $\bar{\eta}$   
122 with high  $\mathcal{I}_{\max}$  are therefore preferred.

123 In Fig. 1g, we compare inferred  $\bar{\eta}$  and  $\mathcal{I}_{\max}$  values across models. Geneformer consistently shows the  
124 greatest robustness to noise: across all tasks, it approaches within 0.5 bits of its asymptotic performance  
125 at fewer than 1,000 UMI per cell. scVI displays similarly low noise sensitivity for three of the four tasks,  
126 but in the protein-abundance task it becomes noise-sensitized at  $\sim 4,000$  UMI per cell. PCA, by con-  
127 trast, shows far greater sensitivity to noise, with  $\bar{\eta}$  values 2.5–12.8-fold larger than those of Geneformer,  
128 consistent with the limited denoising capacity of linear methods.

129 Despite its robustness to noise, Geneformer is not a strong model in terms of its capacity. Across all  
130 tasks, its capacity,  $\mathcal{I}_{\max}$ , is lower than those of scVI by 0.4–1.4 bits – corresponding to approximately  
131 halving the complexity of the captured signal. This difference in performance is not only in its asymptotic  
132 capacity, but also at the noise level present in the datasets (Fig. 1d). Thus, scVI ultimately extracts  
133 more auxiliary information in the limit of low noise. It is possible that other models may simultaneously  
134 show noise robustness and higher information capacity.

**Box 1: A model of noise scaling in representation learning**

The empirical noise–performance curves in Fig. 1d suggest that a simple theoretical relationship underlies how measurement noise limits the information extractable by representation models. A classical setting in which such limits are analytically tractable is a Gaussian noise channel, where both the signal and the noise are modeled as Gaussian random variables. Although simplified, this framework captures the essential effect of diminishing returns: as measurement quality improves, each additional increment in signal-to-noise ratio (SNR) conveys progressively less new information. We use it to derive the scaling form in Eq. (1).

Let  $X, Y$  be multivariate Gaussian random vectors representing the system state and an auxiliary signal, and let  $Z$  be a noisy measurement of  $X$  with SNR  $\eta$ :

$$Y \sim \mathcal{N}(0, \Sigma_Y), \quad X = Y + \mathcal{N}(0, \Sigma_U), \quad Z = \eta X + \mathcal{N}(0, I_n).$$

The mutual information between  $Y$  and  $Z$ —the amount of auxiliary signal retained after measurement—follows the standard expression for Gaussian vector noise channels [31, 33]:

$$I(Y; Z) = \frac{1}{2} \log \frac{\det(\Sigma_Y + \Sigma_U + \eta^{-2} I_n)}{\det(\Sigma_U + \eta^{-2} I_n)}.$$

For the scalar case ( $n = 1$ ), where  $\Sigma_Y = \sigma_Y^2$  and  $\Sigma_U = \sigma_U^2$ ,

$$I(Y; Z) = \frac{1}{2} \log \frac{\eta^2(\sigma_Y^2 + \sigma_U^2) + 1}{1 + \sigma_U^2 \eta^2}. \quad (2)$$

Two characteristic quantities govern this scaling:

$$\mathcal{I}_{\max} = \lim_{\alpha \rightarrow \infty} I(Y; Z) = \frac{1}{2} \log \frac{\sigma_Y^2 + \sigma_U^2}{\sigma_U^2},$$

the maximal achievable information, and  $\bar{\eta} = 1/\sigma_U^2$ , an effective noise scale. Substituting  $\mathcal{I}_{\max}$  and  $\bar{\eta}$  into  $I(Y; Z)$  recovers precisely the empirical noise-scaling relationship of Eq. 1. Despite its simplicity, this model captures the universal shape of the performance–noise curves observed across datasets and architectures.

135

**136 Generalization of noise scaling**

137 The noise scaling observed in single-cell representation learning may extend to other data modalities.  
138 The scaling law (Eq. 1) depends only on the signal-to-noise ratio  $\eta$ , and a model that explains this law  
139 (Box 1) is not specific to transcriptomic data. To test whether this framework generalizes, we examined  
140 whether Eq. 1 quantitatively predicts noise–performance relationships in image representation models,  
141 and then in a protein sequence model.

142 For image representation, we used MobileNetV2, a lightweight convolutional architecture designed  
143 for image classification [34]. We trained and evaluated this model on a 5-class subset of the Caltech101  
144 dataset [35], consisting of  $240 \times 240$  pixel images with 1,354 total images. Images were perturbed with two  
145 distinct forms of degradation: additive Gaussian noise and reduced spatial resolution. Pixel-wise Gaussian  
146 noise is common in imaging measurements [36]. We then used auxiliary-MI to evaluate model performance  
147 under both forms of image noise. As with the transcriptomic models, we quantified performance using

auxiliary-MI, here measuring the mutual information between the learned representations and the true image labels. We trained the MobileNetV2 models and computed the auxiliary-MI between predicted and true labels on held-out images, assessing performance for two tasks: classification of all class labels, as well as multiple one-vs-all problems. We introduced Gaussian noise with  $\eta = 1/\sigma_N^2$ , where  $\sigma_N$  is the noise standard deviation, while resolution degradation was introduced by averaging local pixel neighborhoods, with  $\eta = 1/f$  for downsampling factor  $f$ . Downsampling introduces a noise SNR  $f$ . For both types of noise, we found that Eq. 1 accurately reproduced the observed noise–performance curves for all classification tasks (**Fig. 1h**).

## Noise scaling and experimental design

Measurement noise scaling laws can be used to determine the data quality or sample quantity required to achieve a specified level of representation performance. The parameter  $\bar{\eta}$  from Eq. 1 directly reports the measurement sensitivity at which model performance reaches within 0.5 bits (or approximately 70%) of its asymptotic value. More generally, inverting Eq. 1 yields a function  $\eta(\mathcal{I})$  that predicts the minimum signal-to-noise ratio needed for a model to achieve a desired information content with respect to a given auxiliary variable.

For transcriptomic data,  $\eta$  is proportional to the total UMIs per cell, enabling an estimate of the sequencing depth needed for a representation to reach, for example, 90% of its maximum informativity. Several clear patterns emerge. Geneformer consistently operates below its UMI90 on all datasets examined, indicating that its performance is already near its asymptotic limit under typical sequencing depths. In contrast, UMI90 for scVI exceeds the observed UMI counts for protein abundance, spatial information, and clonal information tasks—suggesting that these tasks remain sensitivity-limited and would benefit from deeper sequencing. These examples illustrate how noise-scaling relationships can guide the choice of models and allocation of sequencing depth across tasks with different intrinsic difficulty.

To assess whether these experimental-design conclusions extend beyond transcriptomics, we applied the same analysis to image representation learning. For image classification (**Fig. 1h**), the fitted  $\mathcal{I}_{\max}$  values closely matched the theoretical maximum determined by the label entropy, and the fitted  $\bar{\eta}$  values provided interpretable design guidance. Certain classes (e.g., “watch”) exhibited a steeper performance decay, indicating that their recognition relies on higher-resolution features. These results parallel the transcriptomic findings and show that noise tolerance thresholds can be used to rationally plan training of image models as well.

## Discussion

Noise in training data inevitably affects model performance, but it has remained unclear whether there exist predictable, quantitative rules governing how representation quality degrades as noise increases.

181 Across single-cell transcriptomics and imaging we find that auxiliary-task performance follows a char-  
182 acteristic sigmoidal scaling curve. Models retain robust performance above a modality-specific noise  
183 threshold, after which representation quality declines approximately logarithmically with increasing noise.  
184 A remarkably simple information-theoretic model captures this relationship and recovers the empirical  
185 scaling form observed across more than  $10^3$  trained representations. These results suggest that predictable  
186 noise-dependent learning curves may be a common feature across diverse biological data modalities.

187 This work provides practical guidance for designing and evaluating biological representation models.  
188 The fitted scaling parameters  $\bar{\eta}$  and  $I_{\max}$  jointly characterize model behavior:  $\bar{\eta}$  reflects noise robustness,  
189 while  $I_{\max}$  represents the maximal task-relevant information that a model can encode. Nonlinear models  
190 such as Geneformer and scVI exhibit substantially greater robustness to measurement noise than PCA,  
191 consistent with the expectation that nonlinear architectures more effectively denoise sparse molecular  
192 measurements. However, robustness alone is insufficient. Geneformer, despite its stability under noise,  
193 often attains a relatively low  $I_{\max}$ , capturing less auxiliary information than scVI and, for certain tasks,  
194 even linear baselines. These results emphasize that noise robustness and representational capacity must  
195 be jointly optimized in model design.

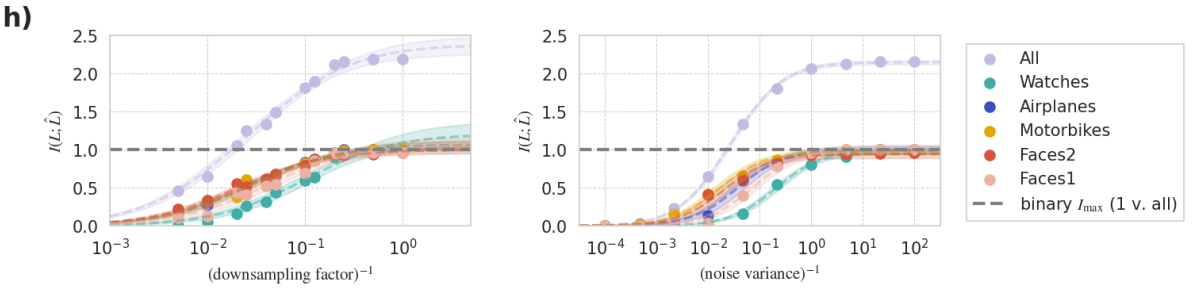
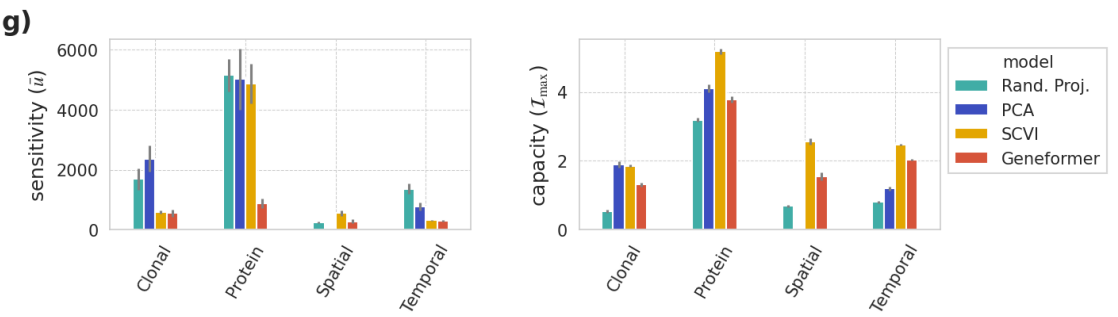
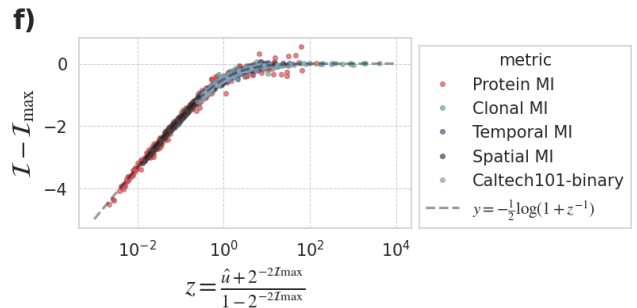
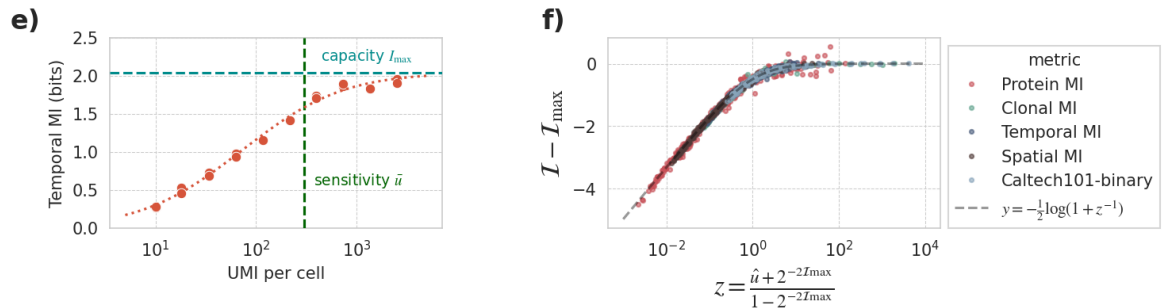
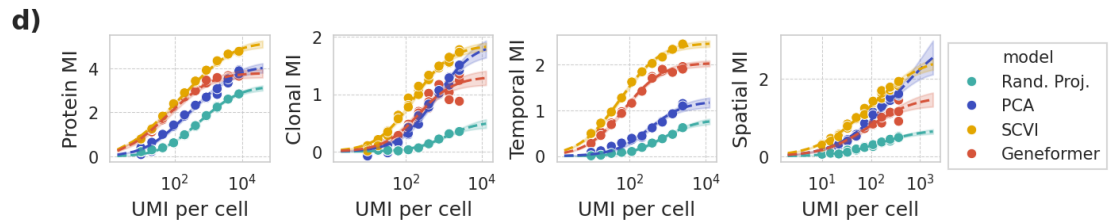
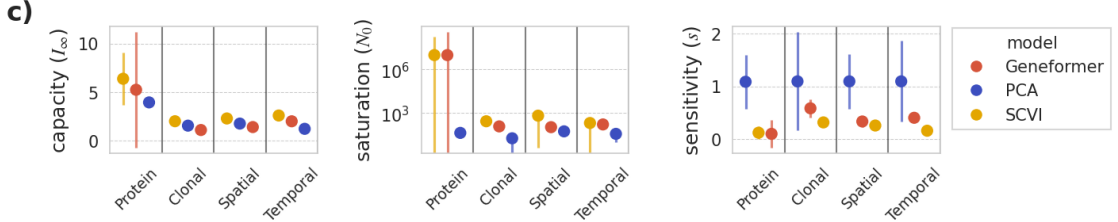
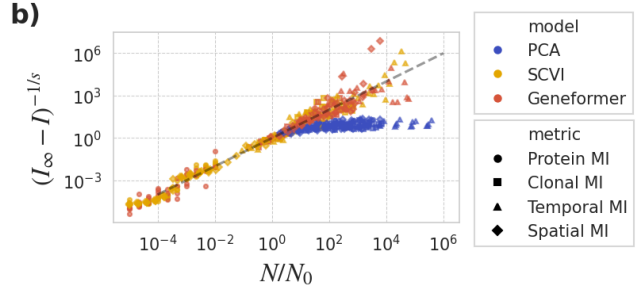
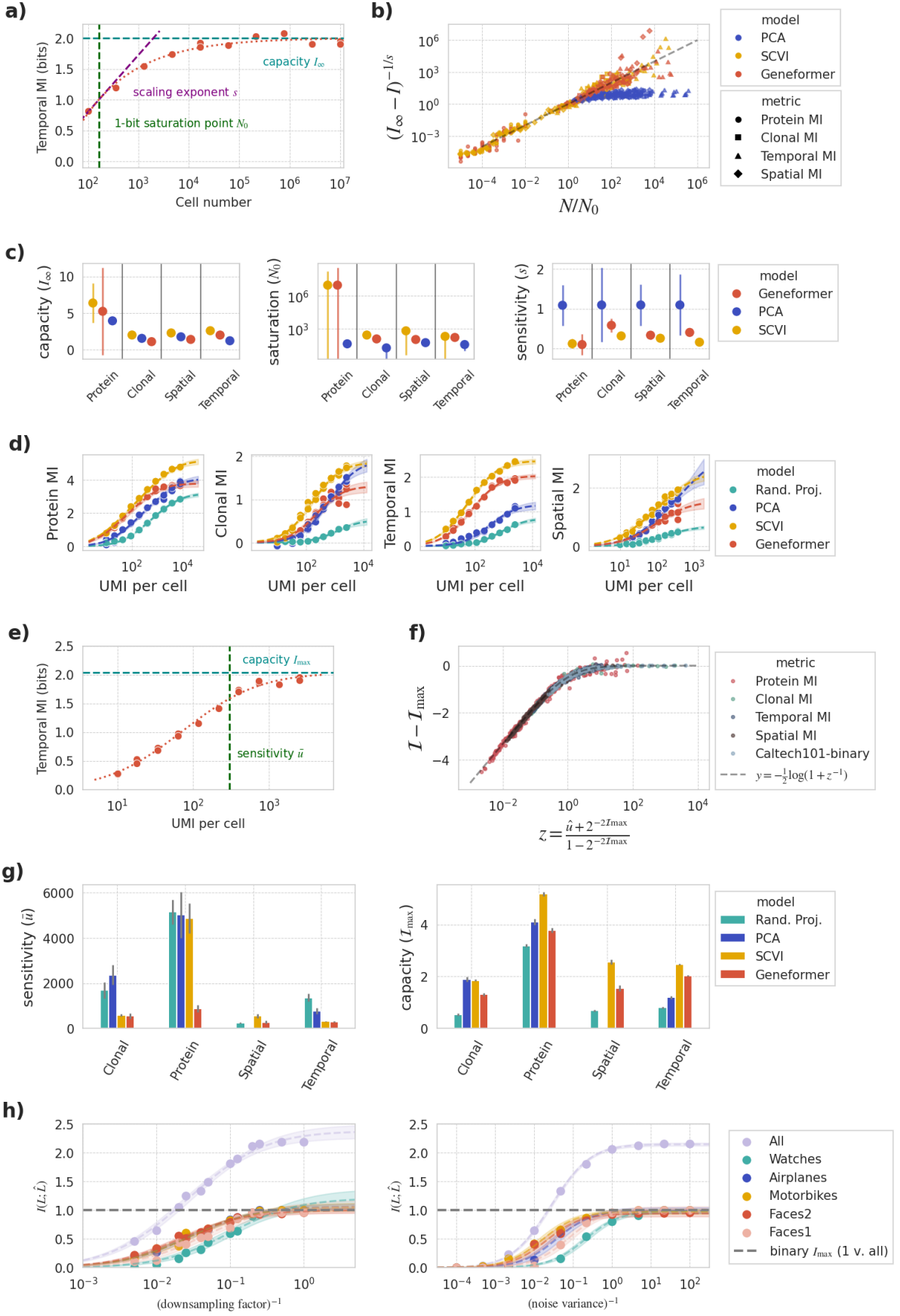
196 Noise scaling has implications for experimental design, particularly for large-scale single-cell profiling.  
197 Our analysis shows that some tasks, such as our test tasks of predicting surface-protein or spatial infor-  
198 mation from scRNA-seq, remain sensitivity-limited even in current datasets. These tasks would benefit  
199 substantially from higher per-cell transcript counts. Conversely, for tasks such as predicting develop-  
200 mental stage in the mouse embryo atlas, existing sequencing depth is already sufficient to approach the  
201 representational limit. These distinctions highlight that improvements in measurement quality, rather  
202 than cell number alone, may be the most impactful direction for next-generation atlases and molecular  
203 profiling initiatives.

204 More broadly, considering measurement noise as an additional scaling axis, parallel to well-established  
205 roles of dataset and model size in neural scaling, suggests a more complete picture of representation  
206 learning in ‘measurement-bound’ fields such as biology. Noise imposes a predictable, quantifiable con-  
207 straint that can be analytically modeled and experimentally manipulated. This creates opportunities for  
208 joint optimization of dataset size and measurement sensitivity, and for designing assays that sit on or  
209 near the optimal learning curve for a given task.

210 Several questions remain. First, we have still only demonstrated noise scaling in a small number of  
211 modeling tasks. Second, even for the tasks at hand, we have only evaluated a small number of model  
212 architectures. The high cost of training modern foundation models makes it impractical for us to evaluate  
213 additional models. It is possible that finetuning of pre-trained models may provide a faithful probe  
214 of noise-tolerances of a model, allowing systematic evaluation of additional models. Third, an open  
215 theoretical question is to understand the origin of the scaling law. The model we introduce here (**Box**

216 1) is exact for scalar Gaussian channels, yet it fits high-dimensional biological data surprisingly well.  
217 Understanding why this is the case, and under what conditions noise scaling breaks down, represents  
218 a theoretical direction. Finally, our analysis has treated measurement noise and sample size separately;  
219 developing a joint scaling law that unifies both axes would further clarify how to allocate resources to  
220 build predictive models of high-dimensional biological systems.

221 In sum, our findings suggest that measurement noise is a predictable and actionable determinant of  
222 representation model performance, one that can be optimized alongside dataset size to guide both model  
223 development and experimental design across biological modalities.



---

Fig. 1 (previous page): **Scaling laws for cellular representation learning.** (a) Geneformer representation quality, measured by information about developmental time, as a function of number of training data points drawn from a mouse embryo development atlas [21]. Theory curve is shown with a dashed line. Cell number scaling parameters  $I_\infty$ ,  $s$ ,  $N_0$  are annotated on the theory curve. (b) Scaling collapse of 54 different cell number scaling curves across three model families and four datasets. Datasets with transcript counts downsampled by more than one order of magnitude are omitted. (c) Comparison of cell number scaling parameters across model families and representation quality metrics. (d) Observations and noise scaling law fits for representation quality as a function of molecules detected per cell. Confidence bands show  $2\sigma$  interval. (e) Geneformer representation quality, measured by information about developmental time, as a function of number of transcripts captured per cell. Theory curve is shown with a dashed line. Noise scaling parameters  $I_{\max}$ ,  $\bar{u}$  are annotated on the theory curve. (f) Scaling collapse of 112 different noise scaling curves across four model families and five datasets. Curves with unconstrained  $I_{\max}$  are omitted. (g) Comparison of noise scaling parameters across model families with fixed-size unsubsamped datasets. Parameters for PCA on the spatial metric are unconstrained and omitted from the plot. (h) Observations and noise scaling law fits for image classification performance of Mobilenetv2 models [34]. Confidence bands show  $2\sigma$  interval.

<sup>224</sup> **Acknowledgements.** This work is supported by funding from NIH Pioneer Award DP1GM133052,  
<sup>225</sup> R01HG012926 to P.Y., and Molecular Robotics Initiative at the Wyss Institute. A.M.K. acknowledges  
<sup>226</sup> support of an Edward Mallinckrodt Jr. Scholar Award.

## <sup>227</sup> References

- <sup>228</sup> [1] Yao, Z., Velthoven, C.T.J., Kunst, M., Zhang, M., McMillen, D., Lee, C., Jung, W., Goldy, J., Abdel-  
<sup>229</sup> hak, A., Aitken, M., Baker, K., Baker, P., Barkan, E., Bertagnolli, D., Bhandiwad, A., Bielstein, C.,  
<sup>230</sup> Bishwakarma, P., Campos, J., Carey, D., Casper, T., Chakka, A.B., Chakrabarty, R., Chavan, S.,  
<sup>231</sup> Chen, M., Clark, M., Close, J., Crichton, K., Daniel, S., DiValentin, P., Dolbeare, T., Ellingwood,  
<sup>232</sup> L., Fiabane, E., Fliss, T., Gee, J., Gerstenberger, J., Glandon, A., Gloe, J., Gould, J., Gray, J., Guil-  
<sup>233</sup> ford, N., Guzman, J., Hirschstein, D., Ho, W., Hooper, M., Huang, M., Hupp, M., Jin, K., Kroll,  
<sup>234</sup> M., Lathia, K., Leon, A., Li, S., Long, B., Madigan, Z., Malloy, J., Malone, J., Maltzer, Z., Martin,  
<sup>235</sup> N., McCue, R., McGinty, R., Mei, N., Melchor, J., Meyerdierks, E., Mollenkopf, T., Moonsman, S.,  
<sup>236</sup> Nguyen, T.N., Otto, S., Pham, T., Rimorin, C., Ruiz, A., Sanchez, R., Sawyer, L., Shapovalova,  
<sup>237</sup> N., Shepard, N., Slaughterbeck, C., Sulc, J., Tieu, M., Torkelson, A., Tung, H., Valera Cuevas, N.,  
<sup>238</sup> Vance, S., Wadhwan, K., Ward, K., Levi, B., Farrell, C., Young, R., Staats, B., Wang, M.-Q.M.,  
<sup>239</sup> Thompson, C.L., Mufti, S., Pagan, C.M., Kruse, L., Dee, N., Sunkin, S.M., Esposito, L., Hawrylycz,  
<sup>240</sup> M.J., Waters, J., Ng, L., Smith, K., Tasic, B., Zhuang, X., Zeng, H.: A high-resolution transcrip-  
<sup>241</sup> tomic and spatial atlas of cell types in the whole mouse brain. *Nature* **624**(7991), 317–332 (2023)  
<sup>242</sup> <https://doi.org/10.1038/s41586-023-06812-z>
- <sup>243</sup> [2] Zhang, J., Ubas, A.A., Borja, R., Svensson, V., Thomas, N., Thakar, N., Lai, I., Winters, A., Khan,  
<sup>244</sup> U., Jones, M.G., Tran, V., Pangallo, J., Papalex, E., Sapre, A., Nguyen, H., Sanderson, O., Nigos,  
<sup>245</sup> M., Kaplan, O., Schroeder, S., Hariadi, B., Marrujo, S., Salvino, C.C.A., Gallareta Olivares, G.,  
<sup>246</sup> Koehler, R., Geiss, G., Rosenberg, A., Roco, C., Merico, D., Alidoust, N., Goodarzi, H., Yu, J.:  
<sup>247</sup> *Tahoe-100M*: A Giga-scale single-cell perturbation atlas for context-dependent gene function and  
<sup>248</sup> cellular modeling. *bioRxiv*, 2025–0220639398 (2025) <https://doi.org/10.1101/2025.02.20.639398>
- <sup>249</sup> [3] Bunne, C., Roohani, Y., Rosen, Y., Gupta, A., Zhang, X., Roed, M., Alexandrov, T., AlQuraishi,  
<sup>250</sup> M., Brennan, P., Burkhardt, D.B., Califano, A., Cool, J., Dernburg, A.F., Ewing, K., Fox, E.B.,  
<sup>251</sup> Haury, M., Herr, A.E., Horvitz, E., Hsu, P.D., Jain, V., Johnson, G.R., Kalil, T., Kelley, D.R., Kelley,  
<sup>252</sup> S.O., Kreshuk, A., Mitchison, T., Otte, S., Shendure, J., Sofroniew, N.J., Theis, F., Theodoris, C.V.,  
<sup>253</sup> Upadhyayula, S., Valer, M., Wang, B., Xing, E., Yeung-Levy, S., Zitnik, M., Karaletsos, T., Regev,  
<sup>254</sup> A., Lundberg, E., Leskovec, J., Quake, S.R.: How to build the virtual cell with artificial intelligence:  
<sup>255</sup> Priorities and opportunities. *arXiv* [q-bio.QM] (2024) [arXiv:2409.11654](https://arxiv.org/abs/2409.11654) [q-bio.QM]

- 256 [4] Wang, H., Leskovec, J., Regev, A.: Limitations of cell embedding metrics assessed using drifting  
islands. *Nature biotechnology*, 1–4 (2025) <https://doi.org/10.1038/s41587-025-02702-z>
- 257
- 258 [5] Gunawan, I., Vafaei, F., Meijering, E., Lock, J.G.: An introduction to representation learning for  
single-cell data analysis. *Cell reports methods* **3**(8), 100547 (2023) <https://doi.org/10.1016/j.crmeth.2023.100547>
- 259
- 260
- 261 [6] Theodoris, C.V., Xiao, L., Chopra, A., Chaffin, M.D., Al Sayed, Z.R., Hill, M.C., Mantineo, H.,  
Brydon, E.M., Zeng, Z., Liu, X.S., Ellinor, P.T.: Transfer learning enables predictions in network  
biology. *Nature* **618**(7965), 616–624 (2023) <https://doi.org/10.1038/s41586-023-06139-9>
- 262
- 263
- 264 [7] Cui, H., Wang, C., Maan, H., Pang, K., Luo, F., Duan, N., Wang, B.: scGPT: toward building a  
foundation model for single-cell multi-omics using generative AI. *Nature methods* **21**(8), 1470–1480  
(2024) <https://doi.org/10.1038/s41592-024-02201-0>
- 265
- 266
- 267 [8] Heimberg, G., Kuo, T., DePianto, D.J., Salem, O., Heigl, T., Diamant, N., Scalia, G., Biancalani,  
T., Turley, S.J., Rock, J.R., Corrada Bravo, H., Kaminker, J., Vander Heiden, J.A., Regev, A.: A  
cell atlas foundation model for scalable search of similar human cells. *Nature*, 1–3 (2024) <https://doi.org/10.1038/s41586-024-08411-y>
- 268
- 269
- 270
- 271 [9] Richter, T., Bahrami, M., Xia, Y., Fischer, D.S., Theis, F.J.: Delineating the effective use of self-  
supervised learning in single-cell genomics. *Nature machine intelligence*, 1–11 (2024) <https://doi.org/10.1038/s42256-024-00934-3>
- 272
- 273
- 274 [10] Hestness, J., Narang, S., Ardalani, N., Diamos, G., Jun, H., Kianinejad, H., Patwary, M.M.A.,  
Yang, Y., Zhou, Y.: Deep Learning Scaling is Predictable, Empirically. *arXiv* [cs.LG] (2017)  
[arXiv:1712.00409](https://arxiv.org/abs/1712.00409) [cs.LG]
- 275
- 276
- 277 [11] Rosenfeld, J.S., Rosenfeld, A., Belinkov, Y., Shavit, N.: A constructive prediction of the generaliza-  
tion error across scales. *arXiv* [cs.LG] (2019) [arXiv:1909.12673](https://arxiv.org/abs/1909.12673) [cs.LG]
- 278
- 279 [12] Kaplan, J., McCandlish, S., Henighan, T., Brown, T.B., Chess, B., Child, R., Gray, S., Radford, A.,  
Wu, J., Amodei, D.: Scaling laws for neural language models. *arXiv* [cs.LG] (2020) [arXiv:2001.08361](https://arxiv.org/abs/2001.08361)  
[cs.LG]
- 280
- 281
- 282 [13] Hoffmann, J., Borgeaud, S., Mensch, A., Buchatskaya, E., Cai, T., Rutherford, E., Casas, D.d.L.,  
Hendricks, L.A., Welbl, J., Clark, A., Hennigan, T., Noland, E., Millican, K., Driessche, G., Damoc,  
B., Guy, A., Osindero, S., Simonyan, K., Elsen, E., Rae, J.W., Vinyals, O., Sifre, L.: Training  
Compute-Optimal Large Language Models. *arXiv* [cs.CL] (2022) [arXiv:2203.15556](https://arxiv.org/abs/2203.15556) [cs.CL]
- 283
- 284
- 285

- 286 [14] Bahri, Y., Dyer, E., Kaplan, J., Lee, J., Sharma, U.: Explaining neural scaling laws. Proceedings  
287 of the National Academy of Sciences of the United States of America **121**(27), 2311878121 (2024)  
288 <https://doi.org/10.1073/pnas.2311878121>
- 289 [15] Chen, D., Zhu, Y., Zhang, J., Du, Y., Li, Z., Liu, Q., Wu, S., Wang, L.: Uncovering neural scaling laws  
290 in molecular Representation Learning. Neural Information Processing Systems **abs/2309.15123**,  
291 1452–1475 (2023) <https://doi.org/10.48550/arXiv.2309.15123> 2309.15123
- 292 [16] Stoler, N., Nekrutenko, A.: Sequencing error profiles of Illumina sequencing instruments. NAR  
293 genomics and bioinformatics **3**(1), 019 (2021) <https://doi.org/10.1093/nargab/lqab019>
- 294 [17] Hagemann-Jensen, M., Ziegenhain, C., Chen, P., Ramsköld, D., Hendriks, G.-J., Larsson, A.J.M.,  
295 Faridani, O.R., Sandberg, R.: Single-cell RNA counting at allele and isoform resolution using Smart-  
296 seq3. Nature biotechnology **38**(6), 708–714 (2020) <https://doi.org/10.1038/s41587-020-0497-0>
- 297 [18] Svensson, V., Natarajan, K.N., Ly, L.-H., Miragaia, R.J., Labalette, C., Macaulay, I.C., Cvejic, A.,  
298 Teichmann, S.A.: Power analysis of single-cell RNA-sequencing experiments. Nature methods **14**(4),  
299 381–387 (2017) <https://doi.org/10.1038/nmeth.4220>
- 300 [19] Lichtman, J.W., Conchello, J.-A.: Fluorescence microscopy. Nature methods **2**(12), 910–919 (2005)  
301 <https://doi.org/10.1038/nmeth817>
- 302 [20] Bansal, Y., Ghorbani, B., Garg, A., Zhang, B., Krikun, M., Cherry, C., Neyshabur, B., Firat,  
303 O.: Data scaling laws in NMT: The effect of noise and architecture. arXiv [cs.LG] (2022)  
304 [arXiv:2202.01994](https://arxiv.org/abs/2202.01994) [cs.LG]
- 305 [21] Qiu, C., Martin, B.K., Welsh, I.C., Daza, R.M., Le, T.-M., Huang, X., Nichols, E.K., Taylor, M.L.,  
306 Fulton, O., O'Day, D.R., Gomes, A.R., Ilcisin, S., Srivatsan, S., Deng, X., Disteche, C.M., Noble,  
307 W.S., Hamazaki, N., Moens, C.B., Kimelman, D., Cao, J., Schier, A.F., Spielmann, M., Murray, S.A.,  
308 Trapnell, C., Shendure, J.: A single-cell time-lapse of mouse prenatal development from gastrula to  
309 birth. Nature **626**(8001), 1084–1093 (2024) <https://doi.org/10.1038/s41586-024-07069-w>
- 310 [22] Brandfonbrener, D., Anand, N., Vyas, N., Malach, E., Kakade, S.: Loss-to-loss prediction: Scaling  
311 laws for all datasets. arXiv [cs.LG] (2024) [arXiv:2411.12925](https://arxiv.org/abs/2411.12925) [cs.LG]
- 312 [23] Belinkov, Y.: Probing classifiers: Promises, shortcomings, and advances. Computational linguistics  
313 (Association for Computational Linguistics) **48**(1), 207–219 (2022) [https://doi.org/10.1162/coli\\_a\\_00422](https://doi.org/10.1162/coli_a_00422)

- 315 [24] Pimentel, T., Valvoda, J., Maudslay, R.H., Zmigrod, R., Williams, A., Cotterell, R.: Information-  
316 theoretic probing for linguistic structure. arXiv [cs.CL] (2020) [arXiv:2004.03061](https://arxiv.org/abs/2004.03061) [cs.CL]
- 317 [25] Gowri, G., Lun, X.-K., Klein, A.M., Yin, P.: Approximating mutual information of high-dimensional  
318 variables using learned representations. In: Globerson, A., Mackey, L., Belgrave, D., Fan, A., Paquet,  
319 U., Tomczak, J., Zhang, C. (eds.) Advances in Neural Information Processing Systems, vol. 37, pp.  
320 132843–132875. Curran Associates, Inc., ??? (2024)
- 321 [26] Hao, Y., Hao, S., Andersen-Nissen, E., Mauck, W.M. 3rd, Zheng, S., Butler, A., Lee, M.J., Wilk, A.J.,  
322 Darby, C., Zager, M., Hoffman, P., Stoeckius, M., Papalex, E., Mimitou, E.P., Jain, J., Srivastava,  
323 A., Stuart, T., Fleming, L.M., Yeung, B., Rogers, A.J., McElrath, J.M., Blish, C.A., Gottardo, R.,  
324 Smibert, P., Satija, R.: Integrated analysis of multimodal single-cell data. *Cell* **184**(13), 3573–358729  
325 (2021) <https://doi.org/10.1016/j.cell.2021.04.048>
- 326 [27] Weinreb, C., Rodriguez-Fraticelli, A., Camargo, F.D., Klein, A.M.: Lineage tracing on transcrip-  
327 tional landscapes links state to fate during differentiation. *Science* **367**(6479) (2020) <https://doi.org/10.1126/science.aaw3381>
- 328 [28] Vizgen: Vizgen Data Release V1.0. Title of the publication associated with this dataset: Mouse  
329 Brain Receptor Map (2021)
- 330 [29] Lopez, R., Regier, J., Cole, M.B., Jordan, M.I., Yosef, N.: Deep generative modeling for  
331 single-cell transcriptomics. *Nature methods* **15**(12), 1053–1058 (2018) <https://doi.org/10.1038/s41592-018-0229-2>
- 332 [30] DenAdel, A., Hughes, M., Thoutam, A., Gupta, A., Navia, A.W., Fusi, N., Raghavan, S., Win-  
333 ter, P.S., Amini, A.P., Crawford, L.: Evaluating the role of pre-training dataset size and diversity  
334 on single-cell foundation model performance. *bioRxiv*, 2024–1213628448 (2024) <https://doi.org/10.1101/2024.12.13.628448>
- 335 [31] Guo, D.: Gaussian channels: Information, estimation and multiuser detection. PhD thesis (2004)
- 336 [32] Klein, A.M., Mazutis, L., Akartuna, I., Tallapragada, N., Veres, A., Li, V., Peshkin, L., Weitz, D.A.,  
337 Kirschner, M.W.: Droplet barcoding for single-cell transcriptomics applied to embryonic stem cells.  
338 *Cell* **161**(5), 1187–1201 (2015) <https://doi.org/10.1016/j.cell.2015.04.044>
- 339 [33] Polyanskiy, Y., Wu, Y.: Information Theory: From Coding to Learning. Cambridge university press,  
340 ??? (2024)
- 341 [34] Sandler, M., Howard, A., Zhu, M., Zhmoginov, A., Chen, L.-C.: MobileNetV2: Inverted residuals

- 345 and linear bottlenecks. arXiv [cs.CV] (2018) [arXiv:1801.04381](https://arxiv.org/abs/1801.04381) [cs.CV]
- 346 [35] Fei-Fei, L., Fergus, R., Perona, P.: Learning generative visual models from few training examples:  
347 An incremental bayesian approach tested on 101 object categories, 178–178 (2004)
- 348 [36] Costa, G.B.P., Contato, W.A., Nazare, T.S., Neto, J.a.E.S.B., Ponti, M.: An empirical study on the  
349 effects of different types of noise in image classification tasks. arXiv [cs.CV] (2016) [arXiv:1609.02781](https://arxiv.org/abs/1609.02781)  
350 [cs.CV]